The role of high-order anharmonicity and off-diagonal terms in thermal conductivity: a case study of multi-phase $CsPbBr_3$

Xiaoying Wang,[1] Zhibin Gao,[1, †] Guimei Zhu[2, *], Jie Ren,[3] Lei Hu[1], Jun Sun,[1] Xiangdong Ding,[1] Yi Xia,[4, ‡] and Baowen Li[5]

[1]State Key Laboratory for Mechanical Behavior of Materials,
Xi'an Jiaotong University, Xi'an 710049, China

[2]School of Microelectronics, Southern University of Science and Technology, Shenzhen, 518055, PR China

[3]Center for Phononics and Thermal Energy Science, China-EU Joint Center for Nanophononics,
Shanghai Key Laboratory of Special Artificial Microstructure Materials and Technology,
School of Physics Sciences and Engineering, Tongji University, Shanghai 200092, China

[4]Department of Mechanical and Materials Engineering,
Portland State University, Portland, Oregon 97201, USA

[5]Department of Materials Science and Engineering,
Department of Physics. Southern University of Science and Technology, Shenzhen,
518055, PR China. International Quantum Academy, Shenzhen 518048,
PR China. Paul M. Rady Department of Mechanical Engineering and Department of Physics,
University of Colorado, Boulder, Colorado 80305-0427, USA

† E-mail: zhibin.gao@xjtu.edu.cn

* E-mail: zhugm@sustech.edu.cn

‡ E-mail: yxia@pdx.edu

DFT calculations were performed using the Vienna ab initio simulation package (VASP) [4] with the projector-augmented wave (PAW) method [5, 6]. Since LDA underestimates the lattice parameters and PBE overestimates them, we used PBEsol to obtain accurate lattice constants within 0.25% error compared with the experimental data [1]. The complete results on different functionals can be found in Fig. S1. Cutoff energy of 400 eV was used with 11 × 11× 11 Monkhorst-Pack k-point grids in structure optimization.

The self-consistent iteration for the convergence criterion was below 10^{-8} eV, and all geometries were optimized by the conjugate-gradient method until none of the residual Hellmann-Feynman forces exceeded 10^{-6} eV/˚A. The optimized lattice constant of cubic $Pm\bar{3}m$ phase (No. 221) is 5.862 Å, in good agreement with the experimental value (a =5.847 Å) [1]. For the *P*4/*mbm* tetragonal phase (No. 127), a=b=8.105 Å, c=5.947 Å, in good agreement with the computed result (a = 8.259 Å, c = 5.897 Å) [7]. While for the Pnma phase (No. 62), a = 8.375 Å, b = 7.969 Å, c = 11.633 Å, in good agreement with the experimental value (a = 8.379 Å, b = 7.965 Å, c = 11.633 Å) [1]. A 2 × 2 × 2 supercell and 3 × 3 × 3 k-points were employed in all finite displacement calculations [8]. The harmonic phonon and interatomic force constants (IFCs) calculations were performed by phonopy [9]. To extract the third- and fourth-order IFCs, we used the Compressive Sensing Lattice Dynamics (CSLD) approach that utilizes the compressive sensing technique [10] to select the physically relevant IFCs from the force-displacement data under the constraints enforced by the space group symmetry. Specifically, CSLD adopts the least absolute shrinkage and selection operator (LASSO) technique to obtain

the sparse solution. In our work, three-phonon (3ph) and four-phonon (4ph) are all considered.

We generated force-displacement data by performing ab initio molecular dynamics (AIMD) simulation with a 2 × 2 × 2 supercell at 300 K for 2000 steps with a time step of 2 fs in NVT ensemble using a Nose-Hoover thermostat and 10^{-6} eV energy threshold. We sampled 40 atomic configurations that were equally spaced in time by skipping the first 400 steps from the trajectories and then randomly displaced all of the atoms within the supercell by 0.02 Å (second-order) and 0.1 Å (higher-order) in random directions in each configuration to decrease cross-correlations in the sensing matrix formed by products of atomic displacements. Finally, the 40 uncorrelated sets were computed using accurate DFT calculations with a 10^{-8} eV energy convergence threshold. The numbers of atoms for P3 (cubic), P2 (tetragonal), and P1 (orthorhombic) are 5, 10, and 20, respectively. The corresponding calculated amount of IFCs increases significantly. Therefore, we adopt different grids to calculate κ_L. For cubic phase, we used 12 × 12 × 12 for κ_p^{3ph}, and 10 × 10 × 10 for $\kappa_p^{3,4ph}$ methods. For the tetragonal phase, 7 × 7 × 7 was adopted for κ_p^{3ph}. We employed a scaling algorithm that has been testified in the literature [11] to deal with situations beyond our current computational capabilities. Therefore, we used the ratio of $\kappa_{3,4ph}/\kappa_{3ph}$ to obtain $\kappa_{3,4ph}$ result of 7 × 7 × 7 in the tetragonal phase. For the orthorhombic phase, we used 6 × 6 × 6 grids for κ_p^{3ph} and 7 × 7 × 7 for the ratio of $\kappa_{3,4ph}/\kappa_{3ph}$ to obtain $\kappa_{3,4ph}$. 6 × 6 × 6 grids were adopted for κc in all phases. The convergence test as a function of grids can be found in Fig. S2.

	Lattice constant, α (Å)	**The difference, δ (Å)**
Experimental data	5.847	0
LDA	5.76075	-0.086244
LDA-D2	5.503424	-0.343576
LDA-D3	4.931556	-0.915444
LDA-optB86b	5.873859	0.026859
LDA-optB88	5.895399	0.048399
LDA-SCAN+rVV10	5.828647	-0.018353
PBE	5.9835997	0.1365997
PBE-D2	5.676794	-0.170206
PBE-D3	5.9110878	0.0640878
PBE-DF2	6.0664116	0.2194116
PBE-optB86B	5.8851352	0.0381352

PBE-optB88	5.906116	0.059116
PBEsol-D2	5.5720531	-0.274947
PBEsol-D3	5.8043236	-0.042676
PBEsol-DF2	6.0664116	0.2194116
PBEsol-optB86b	5.8851352	0.0381352
PBEsol-optB88	5.906116	0.059116
PBEsol	**5.8582863**	**0.0112863**

FIG. S1. Calculated lattice constants using different exchange-correlation functionals compared with the experimental lattice constant at 300 K [1]. $\boldsymbol{\delta}$ is defined by $\boldsymbol{\alpha_{Ecp}}$-$\boldsymbol{\alpha_{Cal.}}$ The function of PBEsol possesses the smallest error, which is selected in this calculation.

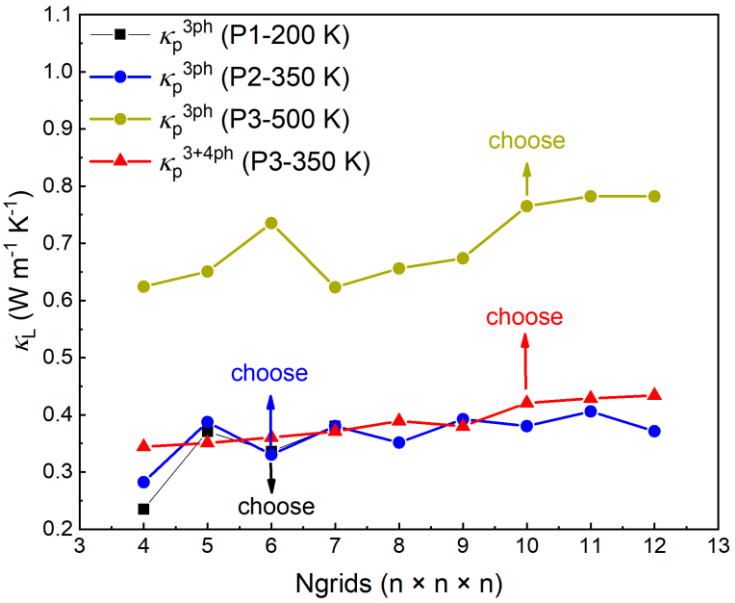

FIG. S2. Convergence test of computation in lattice thermal conductivity for orthorhombic (P1), tetragonal (P2), and cubic (P3) phases, respectively. κ_p and κ_c are the lattice thermal conductivity based on the phonon diagonal terms and off-diagonal terms, relatively. For the P1 phase, due to the current computational capabilities, we adopt 6 × 6 × 6 grids for the κ_p^{3ph} situation (P1-200 K).

Temperature(K)	**Unified theory**	**QP-NL**	κ_p^{3ph}	κ_p^{3+4ph}	κ_c	$\kappa_p^{3ph}+\kappa_c$	$\kappa_p^{3+4ph}+\kappa_c$
50	0.72485		0.53125	0.45534	0.12578	0.65703	0.58112
60	0.66128		0.52001	0.44433	0.13964	0.65965	0.58397
70	0.61733		0.50577	0.43128	0.14819	0.65396	0.57947
80	0.58391		0.48799	0.41353	0.15454	0.64253	0.56807
90	0.55814		0.47089	0.3984	0.15837	0.62926	0.55677
100	0.53542		0.45631	0.3822	0.16093	0.61724	0.54313

110	0.51903		0.44336	0.36534	0.16304	0.6064	0.52838
120	0.50136		0.43221	0.34982	0.16386	0.59607	0.51368
130	0.49103		0.42243	0.33522	0.16457	0.587	0.49978
140	0.47783		0.41021	0.32007	0.16423	0.57444	0.4843
150	0.4696		0.40106	0.30561	0.16422	0.56528	0.46983
160	0.46		0.3911	0.29533	0.16354	0.55464	0.45887
170	0.45306		0.38376	0.28717	0.16295	0.5467	0.45012
180	0.44721		0.37742	0.27934	0.16258	0.53999	0.44192
190	0.44265		0.37	0.27075	0.16177	0.53177	0.43252
200	0.43967		0.36358	0.2624	0.16145	0.52502	0.42385
210	0.43429		0.35818	0.25374	0.161	0.51918	0.41473
220	0.42957		0.35373	0.24682	0.16075	0.51447	0.40756
230	0.42727		0.34966	0.2418	0.16013	0.50979	0.40193
240	0.42379		0.34515	0.23549	0.16002	0.50516	0.3955
250	0.42063		0.34187	0.22967	0.1595	0.50137	0.38918
260	0.41813		0.33812	0.22663	0.1589	0.49701	0.38552
270	0.41636		0.33437	0.2239	0.1588	0.49316	0.3827
280	0.41388		0.33144	0.21946	0.15863	0.49008	0.3781
290	0.41069		0.32778	0.21499	0.158	0.48578	0.37299
300	0.40966		0.32563	0.21151	0.15798	0.48517	0.37096
310（P1）	0.40722		0.32337	0.20773	0.15798	0.48135	0.36229
320（P1）	0.40655		0.32142	0.20431	0.15768	0.4791	0.36199
300（P2）			0.56668	0.37385	0.13993	0.70661	0.51378
305（P2）			0.55563	0.36868	0.13967	0.6953	0.50835
310（P2）			0.54663	0.36356	0.13943	0.68607	0.50299
315（P2）			0.55064	0.35883	0.13931	0.68995	0.49813
320（P2）			0.54663	0.35417	0.13921	0.68584	0.49338
325			0.54203	0.35203	0.13916	0.68119	0.49119
330			0.53769	0.3503	0.13911	0.6768	0.48941
335			0.53345	0.34675	0.13899	0.67244	0.48574
340			0.52927	0.34282	0.13887	0.66813	0.48168
345			0.52466	0.34067	0.13873	0.66339	0.4794
350			0.52037	0.34058	0.13869	0.65906	0.47927
355			0.51589	0.33758	0.1385	0.65439	0.47608
360			0.51241	0.33447	0.13846	0.65087	0.47293
365			0.50828	0.33104	0.13839	0.64667	0.46943
370			0.5045	0.32886	0.13837	0.64287	0.46723
375			0.49977	0.32335	0.13842	0.6382	0.46177
380			0.49524	0.31904	0.13831	0.63355	0.45735
385			0.49182	0.31742	0.13833	0.63015	0.45575
390			0.48811	0.31719	0.13838	0.62648	0.45557
395			0.4849	0.31496	0.13834	0.62324	0.4533
400 (P2)			0.48083	0.31236	0.1384	0.61923	0.45076

410 (P2)			0.47252	0.30761	0.13834	0.61086	0.44595
420 (P2)			0.46583	0.30236	0.13826	0.60409	0.44062
430 (P2)			0.45973	0.29627	0.13848	0.59821	0.43475
440 (P2)			0.45447	0.28897	0.13825	0.59272	0.42723
450 (P2)			0.44805	0.2803	0.13813	0.58618	0.41843
400 (P3)			0.82969	0.43413	0.0798	0.90949	0.51392
450 (P3)			0.80679	0.43226	0.08198	0.88877	0.51424
500			0.78222	0.42085	0.08397	0.86619	0.50482
550			0.76893	0.41461	0.08674	0.85567	0.50135
600			0.76108	0.40569	0.09101	0.85209	0.4967
650			0.74847	0.39012	0.09289	0.84136	0.48301
700			0.73306	0.38616	0.09646	0.82952	0.48262
750			0.72272	0.38022	0.09652	0.81923	0.47673
800			0.71121	0.36075	0.09372	0.80493	0.45447
339.94		0.45149					
360.31		0.47637					
380.23		0.49045					
401.46		0.50238					
420.48		0.50674					
441.26		0.51326					
460.72		0.51331					
480.6		0.50795					
500.93		0.50475					
521.26		0.4994					
541.59		0.49512					
561.48		0.48761					
581.36		0.48009					
602.13		0.47365					
621.56		0.4575					
641		0.44566					
661.76		0.43167					
682.96		0.41551					
701.5		0.39936					
722.26		0.38752					
742.14		0.37353					
761.57		0.36061					
781.89		0.34337					
799.56		0.33477					

FIG. S3. Calculated lattice thermal conductivity compared with the unified theory [2] from Simoncelli, Marzari, and Mauri and the quasiparticle nonlinear theory (QP-NL) [3] from Tadano and Saidi. The units of all thermal conductivity in the table are W m^{-1} K^{-1}.

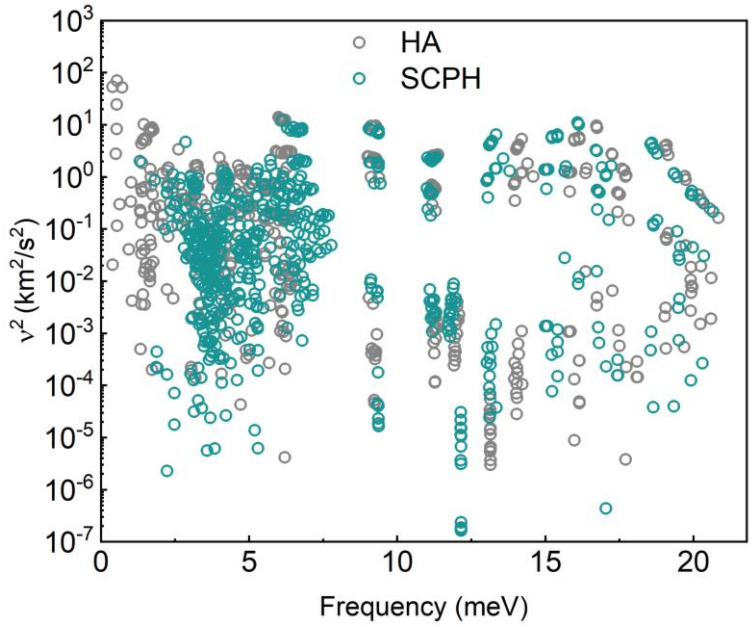

FIG. S4. Two kinds of phonon group velocities containing HA and SCPH for cubic phase at 500 K. HA stands for the calculation of harmonic phonon that fails to consider the temperature effect. SCPH is phonon group velocity calculation under the self-constant phonon approximation.

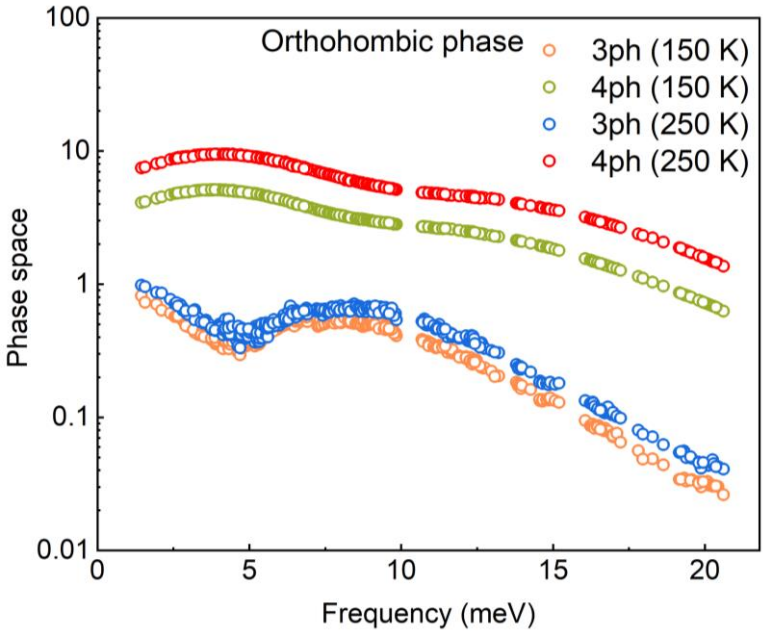

FIG. S5. Calculated phase space compared the four-phonon and three-phonon for the orthorhombic phase at 150 K and 250 K, respectively. With the temperature increasing, the phase space increases accordingly. It is worth noticing that 4ph is more sensitive to the temperature of phase space than the 3ph situation.

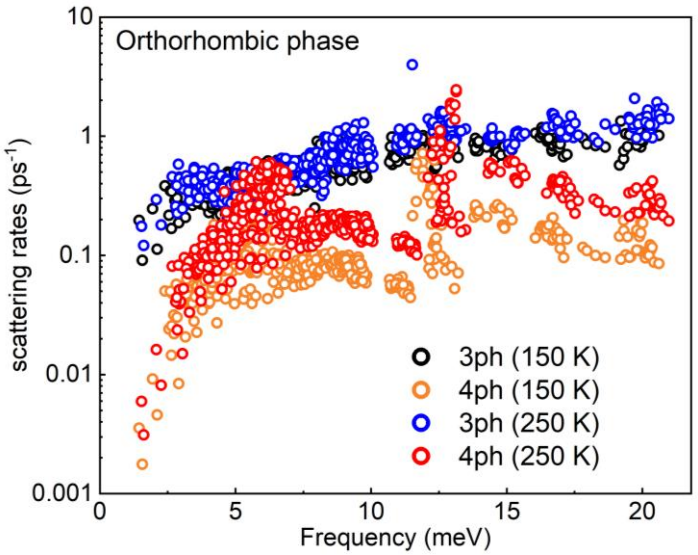

FIG. S6. Calculated phonon scattering rates compared with the four-phonon and three-phonon for the orthorhombic phase at 150 K and 250 K, respectively. The scattering rates increase with increasing temperature. We notice that the 3ph and 4ph are of the same order of magnitude. However, 4ph is more sensitive to the temperature of scattering rates than the 3ph situation.

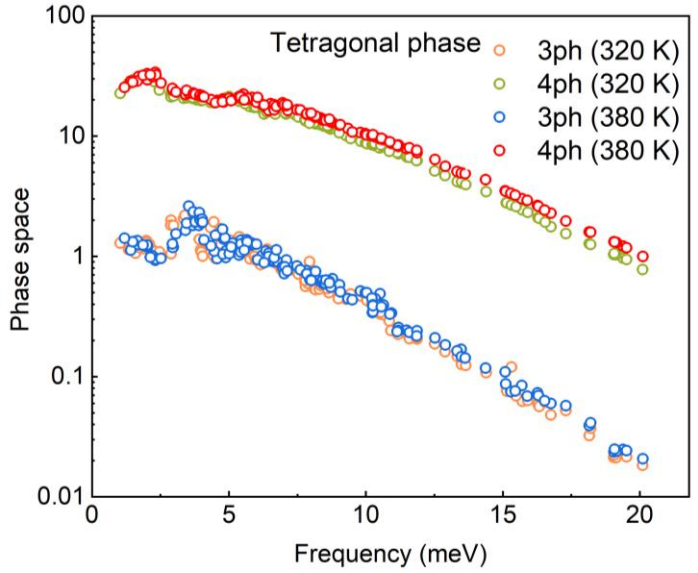

FIG. S7. Calculated phase space compared with four-phonon and three-phonon for the tetragonal phase at 320 K and 380 K, respectively. With the temperature increasing, the phase space increases accordingly. It is worth noticing that 4ph is more sensitive to the temperature of phase space than the 3ph situation.

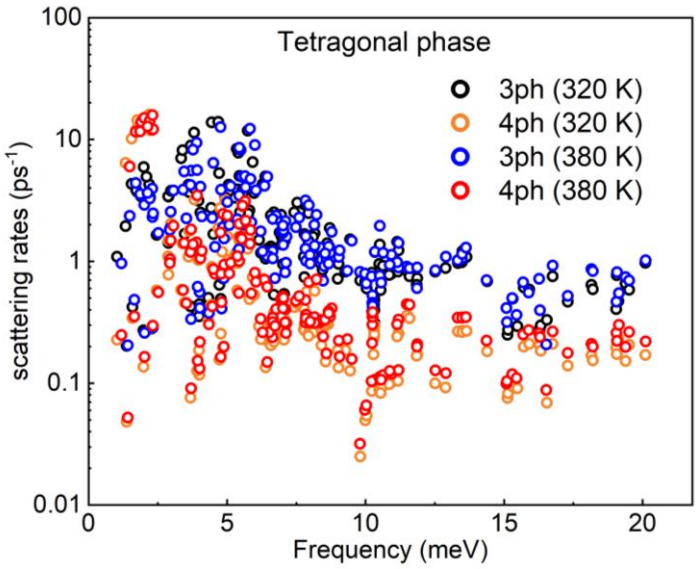

FIG. S8. Calculated phonon scattering rates compared with the four-phonon and three-phonon for the tetragonal phase at 320 K and 380 K, respectively. The scattering rates increase with increasing temperature. We notice that the 3ph and 4ph are of the same order of magnitude. However, 4ph is more sensitive to the temperature of scattering rates than the 3ph situation.

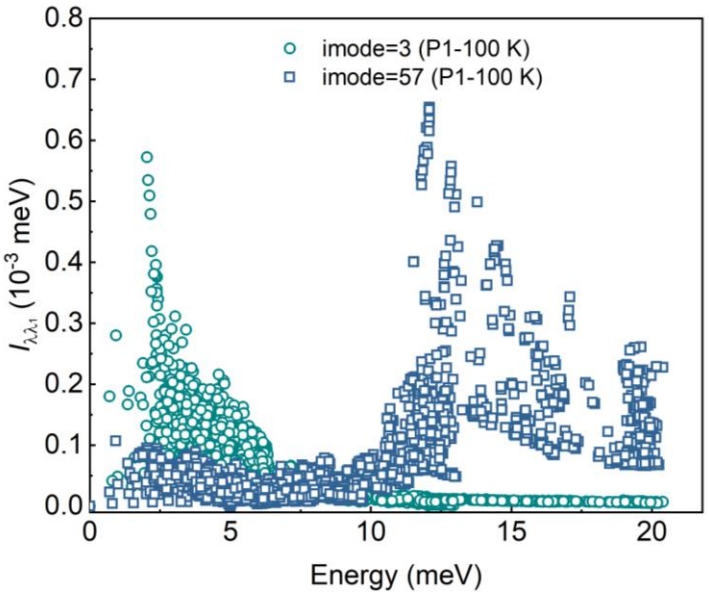

FIG. S9. Matrix parameters for the phonon-phonon interaction of the third acoustic branch (highest frequency acoustic branch imode=3) and the 57th optical branch (imode=57) associated with the strength of the four-phonon interaction matrix elements ($I_{\lambda\lambda 1}$) at 100 K for orthorhombic phase (P1).

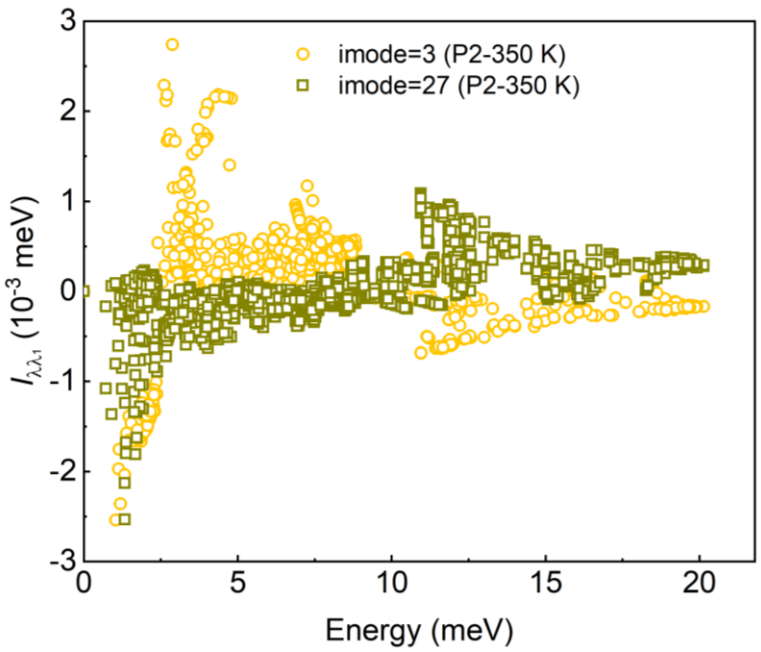

FIG. S10. Matrix parameters for the phonon-phonon interaction of the third acoustic branch (highest frequency acoustic branch imode=3) and the 27th optical branch (imode=27) associated with the strength of the four-phonon interaction matrix elements ($I_{\lambda\lambda 1}$) at 350 K for tetragonal phase (P2).

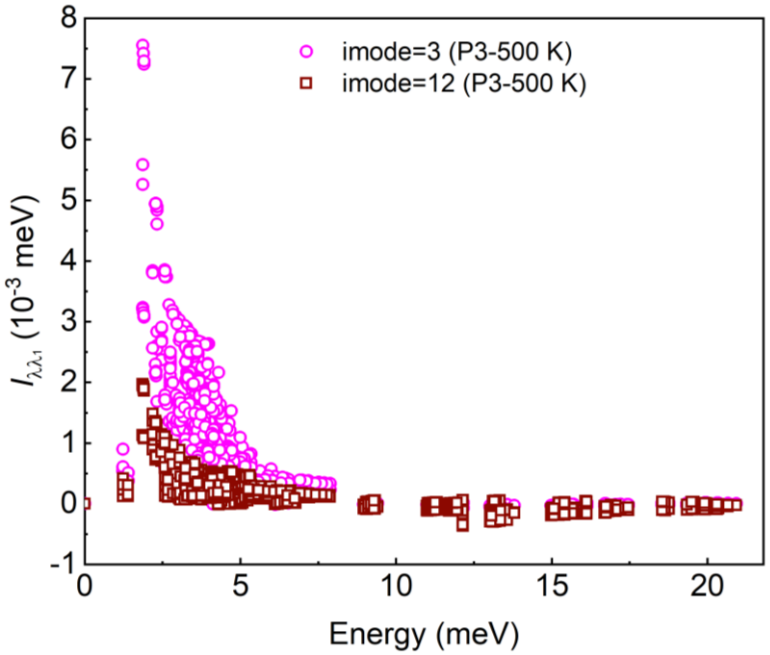

FIG. S11. Matrix parameters for the phonon-phonon interaction of the third acoustic branch (highest frequency acoustic branch imode=3) and the 12th optical branch (imode=12) associated with the strength of the four-phonon interaction matrix elements ($I_{\lambda\lambda 1}$) at 500 K for cubic phase (P3).

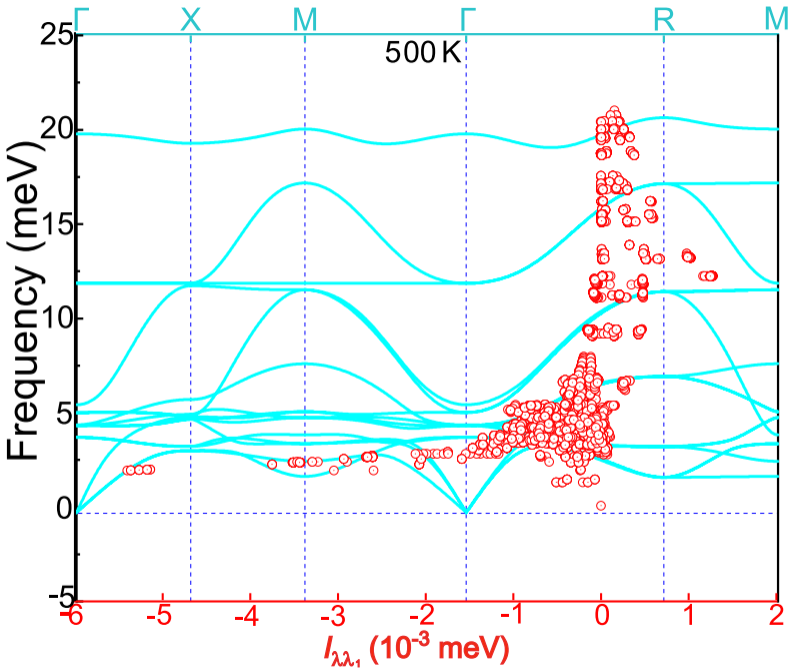

FIG. S12. Matrix parameters for the interaction of the highest optical branch and other phonon frequencies at 500 K for the cubic phase compared with phonon frequency.

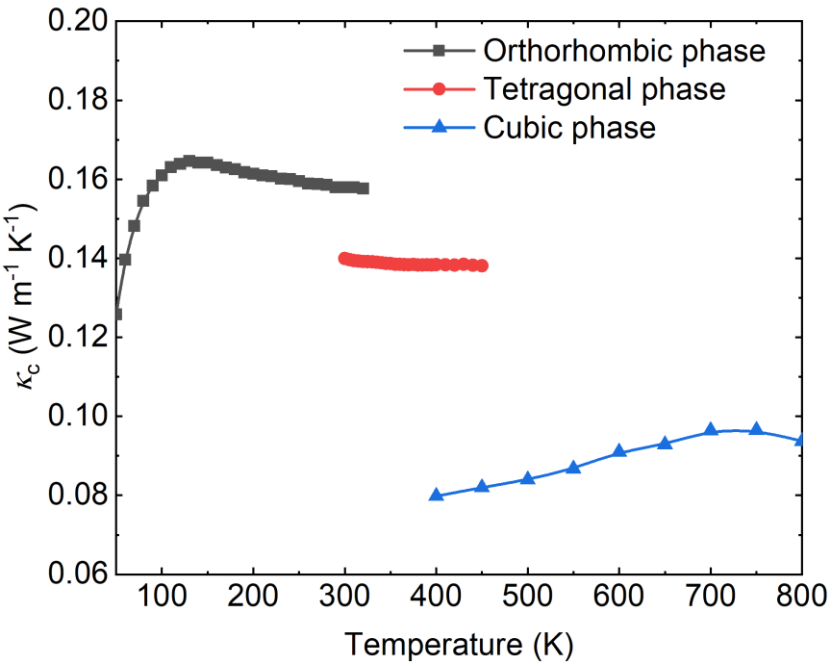

FIG. S13. Lattice thermal conductivity from the off-diagonal term contribution for three phases.

References:

[1] Natarajan, M. and Prakash, B. *Phys. Stat. Sol. (a)* **4,** K167–K172 (1971).
[2] M. Simoncelli, N. Marzari, and F. Mauri, *Nat. Phys.* **15,** 809 (2019).
[3] T. Tadano and W. A. Saidi, *Phys. Rev. Lett.* **129,** 185901 (2022).

[4] G. Kresse and J. Furthmuller, *Phys. Rev. B* **54,** 11169-11186 (1996).
[5] P. E. Blochl, *Phys. Rev. B* **50,** 17953-17979 (1994).
[6] G. Kresse and D. Joubert, *Phys. Rev. B* **59,** 1758-1775 (1999).
[7] T. Lanigan-Atkins, X. He, M. J. Krogstad, D. M. Pajerowski, D. L. Abernathy, G. N. M. N. Xu, Z. Xu, D.-Y. Chung, M. G. Kanatzidis, S. Rosenkranz, R. Osborn, and O. Delaire, *Nat. Mater.* **20,** 977 (2021).
[8] K. Esfarjani and H. T. Stokes, *Phys. Rev. B* **77,** 144112 (2008).
[9] A. Togo and I. Tanaka, *Scripta Materialia* **108,** 1-5 (2015).
[10] E. J. Candes and M. B. Wakin, *IEEE Signal Processing Magazine* **25,** 21 (2008).
[11] Y. Xia, Xia, *Appl. Phys. Lett.* **113,** 073901 (2018).